

Toward a Genome Scale Dynamic Model of Cell Free Protein Synthesis in *Escherichia coli*

Nicholas Horvath, Michael Vilkhovoy, Che-Hsiao Shih¹, Joseph Wayman, Kara Calhoun², James Swartz² and Jeffrey D. Varner*

School of Chemical and Biomolecular Engineering
Cornell University, Ithaca NY 14853

¹School of Chemical Engineering
Purdue University, Lafayette, IN 47901

²School of Chemical Engineering
Stanford University, Stanford, CA 94305

Running Title: Dynamic modeling of cell free protein synthesis

To be submitted: *Scientific Reports*

*Corresponding author:

Jeffrey D. Varner,
Professor, School of Chemical and Biomolecular Engineering,
244 Olin Hall, Cornell University, Ithaca NY, 14853

Email: jdv27@cornell.edu

Phone: (607) 255 - 4258

Fax: (607) 255 - 9166

Abstract

Cell free protein expression systems have become widely used in systems and synthetic biology. In this study, we developed an ensemble of dynamic *E. coli* cell free protein synthesis (CFPS) models. Model parameters were estimated from measurements of glucose, organic acids, energy species, amino acids and the protein product, chloramphenicol acetyltransferase (CAT). The ensemble described the training data, with the exception of some of the amino acid dynamics. To gauge the performance of the cell free reaction, we compared the observed CAT carbon yield, with the maximum theoretical CAT carbon yield calculated using sequence specific flux balance analysis. The observed CAT yield was 45% of the maximum theoretical yield, suggesting CAT production could be further optimized. The metabolic flux distribution predicted by the dynamic model and flux balance analysis were significantly different. The ensemble of dynamic models predicted the majority of carbon flux was routed through glycolysis and the TCA cycle, while flux balance analysis predicted significant flux through the Entner-Doudoroff pathway. Local and global sensitivity analysis suggested CAT production was most sensitive to parameters and initial conditions directly associated with CAT synthesis, as well as GTP/GMP synthesis, amino acid synthesis, and to a lesser extent amino acid initial conditions. On the other hand, CAT production was robust to allosteric control parameters and the initial conditions of glucose and oxygen. Taken together, we presented the first dynamic model of *E. coli* cell free protein synthesis. This study provides a foundation for genome-scale, dynamic modeling of cell-free *E. coli* protein synthesis.

Keywords: Biochemical engineering, systems biology, cell free protein synthesis

1 Introduction

2 Cell-free systems offer many advantages for the study, manipulation and modeling of
3 metabolism compared to *in vivo* processes. Central amongst these advantages is direct
4 access to metabolites and the microbial biosynthetic machinery without the interference of
5 a cell wall. This allows us to control as well as interrogate the chemical environment while
6 the biosynthetic machinery is operating, potentially at a fine time resolution. Second,
7 cell-free systems also allow us to study biological processes without the complications
8 associated with cell growth. Cell-free protein synthesis (CFPS) systems are arguably the
9 most prominent examples of cell-free systems used today [1]. However, CFPS is not new;
10 CFPS in crude *E. coli* extracts has been used since the 1960s to explore fundamentally
11 important biological mechanisms [2, 3]. Today, cell-free systems are used in a variety of
12 applications ranging from therapeutic protein production [4] to synthetic biology [5]. Inter-
13 estingly, many of the challenges confronting genome-scale kinetic modeling can poten-
14 tially be overcome in a cell-free system. For example, there is no complex transcriptional
15 regulation to consider, transient metabolic measurements are easier to obtain, and we
16 no longer have to consider cell growth. Thus, cell-free operation holds several significant
17 advantages for model development, identification and validation. Theoretically, genome-
18 scale cell-free kinetic models may be possible for industrially important organisms, such
19 as *E. coli* or *B. subtilis*, if a simple, tractable framework for integrating allosteric regulation
20 with enzyme kinetics can be formulated.

21 Mathematical modeling has long contributed to our understanding of metabolism. Decades
22 before the genomics revolution, mechanistically, structured metabolic models arose from
23 the desire to predict microbial phenotypes resulting from changes in intracellular or extra-
24 cellular states [6]. The single cell *E. coli* models of Shuler and coworkers pioneered the
25 construction of large-scale, dynamic metabolic models that incorporated multiple, regu-
26 lated catabolic and anabolic pathways constrained by experimentally determined kinetic

parameters [7]. Shuler and coworkers generated many single cell kinetic models, including single cell models of eukaryotes [8, 9], minimal cell architectures [10], as well as DNA sequence based whole-cell models of *E. coli* [11]. Conversely, highly abstracted kinetic frameworks, such as the cybernetic framework, represented a paradigm shift, viewing cells as growth-optimizing strategists [12]. Cybernetic models have been highly successful at predicting metabolic choice behavior, e.g., diauxie behavior [13], steady-state multiplicity [14], as well as the cellular response to metabolic engineering modifications [15]. Unfortunately, traditional, fully structured cybernetic models also suffer from an identifiability challenge, as both the kinetic parameters and an abstracted model of cellular objectives must be estimated simultaneously. However, recent cybernetic formulations from Ramkrishna and colleagues have successfully treated this identifiability challenge through elementary mode reduction [16, 17].

In the post genomics world, large-scale stoichiometric reconstructions of microbial metabolism popularized by static, constraint-based modeling techniques such as flux balance analysis (FBA) have become standard tools [18]. Since the first genome-scale stoichiometric model of *E. coli*, developed by Edwards and Palsson [19], well over 100 organisms, including industrially important prokaryotes such as *E. coli* [20] or *B. subtilis* [21], are now available [22]. Stoichiometric models rely on a pseudo-steady-state assumption to reduce unidentifiable genome-scale kinetic models to an underdetermined linear algebraic system, which can be solved efficiently even for large systems. Traditionally, stoichiometric models have also neglected explicit descriptions of metabolic regulation and control mechanisms, instead opting to describe the choice of pathways by prescribing an objective function on metabolism. Interestingly, similar to early cybernetic models, the most common metabolic objective function has been the optimization of biomass formation [23], although other metabolic objectives have also been estimated [24]. Recent advances in constraint-based modeling have overcome the early shortcomings of

the platform, including capturing metabolic regulation and control [25]. Thus, modern constraint-based approaches have proven extremely useful in the discovery of metabolic engineering strategies and represent the state of the art in metabolic modeling [26, 27]. However, genome-scale kinetic models of industrial important organisms such as *E. coli* have yet to be constructed.

In this study, we developed an ensemble of *E. coli* cell free protein synthesis (CFPS) models using the hybrid cell free modeling approach of Wayman et al [REFHERE]. Model parameters were estimated from measurements of glucose, organic acids, energy species, amino acids and the protein product, chloramphenicol acetyltransferase (CAT). The ensemble described the training data, with the exception of some of the amino acid dynamics. To gauge the performance of the cell free reaction, we compared the observed CAT carbon yield, with the maximum theoretical CAT carbon yield calculated using sequence specific flux balance analysis. The observed CAT yield was 45% of the maximum theoretical yield, suggesting CAT production could be further optimized. The metabolic flux distribution predicted by the dynamic model and flux balance analysis were significantly different. The ensemble of dynamic models predicted the majority of carbon flux was routed through glycolysis and the TCA cycle, while flux balance analysis predicted significant flux through the Entner-Doudoroff pathway. Local and global sensitivity analysis suggested CAT production was most sensitive to parameters and initial conditions directly associated with CAT synthesis, as well as GTP/GMP synthesis, amino acid synthesis, and to a lesser extent amino acid initial conditions. On the other hand, CAT production was robust to allosteric control parameters and the initial conditions of glucose and oxygen. Taken together, we presented the first dynamic model of *E. coli* cell free protein synthesis. We integrated traditional kinetics with a logical rule-based description of allosteric control to simulate a comprehensive CFPS dataset. This study provides a foundation for genome-scale, dynamic modeling of cell-free *E. coli* protein synthesis.

Results

Estimation of an ensemble of cell free protein synthesis models. We used the hybrid cell free modeling framework of Wayman et al. to simulate the production of a model protein [REFHERE]. The cell-free *E. coli* metabolic model was constructed by removing the growth-associated processes from the model of Palsson and coworkers [19], and by adding reactions for the synthesis of chloramphenicol acetyltransferase (CAT), a model protein for which we have a comprehensive training dataset [28]. Thus, the model described core central carbon metabolism (glycolysis, pentose phosphate, Enter-Doudoroff, TCA cycle), as well as the synthesis of energy species, amino acids biosynthesis and degradation, and biosynthesis of the CAT protein. An ensemble of model parameters was estimated from dynamic measurements of glucose, CAT, organic acids (pyruvate, lactate, acetate, succinate, malate), energy species (A(x)P, G(x)P, C(x)P, U(x)P), and 18 of the 20 proteinogenic amino acids. We generated an ensemble of $N = 18,000$ parameter sets by minimizing the error between the training dataset and the metabolite concentrations predicted by the model. We defined the set with the lowest error value as the best-fit parameter set. [STATISTICS ON PARAMETERS].

The ensemble of models captured the time evolution of cell free CAT biosynthesis (Fig. 3 - 7). Glucose was exhausted with 3 hr [FILL ME IN]. The ensemble also captured the energy species dynamics, particularly the overall energy total (Fig. 3, top) and the totals by base . The ensemble and the best-fit set also predict some of the amino acid measurements, while failing to predict others (Fig. 7). the central carbon metabolism, including glucose uptake, CAT production, and the dynamics of the organic acid intermediates . Allosteric control is important to the dynamics of the organic acid intermediates, as without it several of the measurements are not captured by the ensemble or the best-fit set (Fig. 3, bottom). This is likely due to a structural deficiency in the model; in some cases, the consumption of an amino acid through CAT synthesis is not enough to ex-

plain the decrease shown in the data, and there are no other reactions that consume it. Thus, a more comprehensive biological description is needed to fully explain amino acid dynamics.

Maximum theoretical CAT yield showed CFPS can be optimized. We calculated the carbon yield of CAT production for our experimental data and our best-fit parameter set as a function of the initial and final concentrations and the carbon numbers of CAT, glucose, and amino acids. The experimental data displayed a CAT yield of 0.0865, while the best-fit parameter set displayed a CAT yield of 0.0871. While the model ensemble described the experimental data, it was unclear whether the performance of the CFPS system was optimal. To address this question, we used ssFBA in combination with the cell-free metabolic network and a detailed promoter model under a T7 polymerase to compute the maximum theoretical carbon yield. However, we first validated the ssFBA approach by comparing an ensemble of simulated versus measured concentrations of CAT over a one hour period (Fig. 1A). The ensemble of 100 sets captured the CAT concentration profile which was randomly generated by sampling RNA polymerase levels, ribosome levels and elongation rates in a physiological range. We then used sequence-specific FBA to calculate a theoretical maximum CAT yield under four different cases: unconstrained, limited oxidative phosphorylation, bounded by transcription/translation rates, and bounded by experimental data (Fig. 1B). The theoretical maximum carbon yield of CAT was 0.349 for an unconstrained case and 0.194 for the transcription and translation constrained case. Thus, we showed that our experimental dataset and best-fit parameter set were each producing CAT at 25% of the theoretical maximum and 45% of a theoretical physiological case. Whereas, the case constrained by experimental data had a carbon yield of 0.062 ± 0.02 , similar to the experimental yield. This allowed us to quantify the amount of carbon being diverted to byproducts, and suggests that there is potential for a doubling of CAT production by reducing this diversion of carbon. In comparing the flux distributions between the

unconstrained and constrained cases (Fig. 2), both constrained cases heavily utilize the Entner–Doudoroff pathway which may be a first viable knockout to increase CAT yield.

Sensitivity analysis We conducted a local sensitivity analysis to determine which of the kinetic and control parameters affected model performance. We calculated performance as area under the CAT curve, which was directly related to CAT synthesis rate, as the culture time was fixed and no CAT degradation was modeled. We randomly chose 180 sets of the 18,000 sets in the ensemble and defined these as our sub-ensemble; for each set in the sub-ensemble, we varied the rate constant and saturation constants of each metabolic flux and measured the resulting change in CAT production to estimate the sensitivity of model performance to that parameter. We did the same for the control parameters, both the order (Hill coefficient) and gain (related to the the dissociation constant). This allowed us to estimate the relative importance of the kinetic and control parameters to CAT production across the ensemble. Of the rate constants, those with the highest positive sensitivities were CAT synthesis, GTP synthesis, GMP synthesis, glutamine synthesis, and aspartate synthesis (Fig. ??, top). This is explained by GTP and the amino acids being reactants for CAT synthesis. Also, GMP synthesis increases the total amount of guanosine, allowing for more GTP production. The rate constants with the largest negative sensitivities were GTP degradation, arginine synthesis, and UMP synthesis. While GTP degradation is obvious, the others can be explained in that they consume ATP as well as several amino acids, all of which are reactants for CAT synthesis. Of the saturation constants, the reverse is seen: the largest positive sensitivities are those associated with arginine synthesis, while the largest negative sensitivities are those associated with CAT synthesis, GTP synthesis, and GMP synthesis (Fig. ??, middle). This is because an increase in saturation constant causes a decrease in the corresponding reaction rate. The control parameters were seen to be the least significant and the most uncertain (Fig. ??, bottom). Only two had a small standard error across the ensemble, relative to the en-

semble mean sensitivity: the gain and order for pyruvate acting as an inhibitor on the pdh reaction. This could be because pdh consumes pyruvate and diverts carbon away from the pathways that ultimately contribute to CAT production. Taken together with the lack of change in glucose uptake and CAT production when control is removed (Fig. 3), this suggests that allosteric control is not the limiting factor to CAT production.

We conducted a global sensitivity analysis on the parameters that could be controlled experimentally: the initial conditions of glucose, oxygen, amino acids, and enzymes. We used the variance-based method of Sobol, and the same objective function of area under the CAT curve. Using a parameter set of relatively good fit against data, we defined parameter bounds and generated a Sobol sequence of 111,600 parameter values that fit within those bounds. We then calculated the total-order sensitivity and confidence interval for each of the experimentally controllable initial conditions. As the sensitivities were total-order, they were guaranteed to be non-negative. The largest sensitivities belonged to the initial conditions of the CAT macromolecular synthesis machinery, GTP synthase, GTP degradation, some amino acids such as phenylalanine, proline, and leucine, and some amino acid synthases (Fig. ??). This is all explained by GTP and amino acids being reactants for CAT synthesis. While some of the amino acids and amino acid synthases were among the highest in sensitivity, theirs were also very uncertain relative to the CAT macromolecular synthesis machinery and GTP synthase. The initial conditions of glucose and oxygen were among the least important according to the global sensitivity analysis, suggesting that the model predicts that CAT production can be sustained by consuming initial stores or can be powered by other means.

Sensitivity analysis on FBA system We conducted global sensitivity on certain fluxes' upper bounds within a constraint-based FBA system, with protein export rate as the objective function.

Discussion

In this study, we developed an ensemble of *E. coli* cell free protein synthesis (CFPS) models using the hybrid cell free modeling approach of Wayman et al [REFHERE]. Model parameters were estimated from measurements of glucose, organic acids, energy species, amino acids and the protein product, chloramphenicol acetyltransferase (CAT). The ensemble described the training data, with the exception of some of the amino acid dynamics. To gauge the performance of the cell free reaction, we compared the observed CAT carbon yield, with the maximum theoretical CAT carbon yield calculated using sequence specific flux balance analysis. The observed CAT yield was 45% of the maximum theoretical yield, suggesting CAT production could be further optimized. The metabolic flux distribution predicted by the dynamic model and flux balance analysis were significantly different. The ensemble of dynamic models predicted the majority of carbon flux was routed through glycolysis and the TCA cycle, while flux balance analysis predicted significant flux through the Entner-Doudoroff pathway. Local and global sensitivity analysis suggested CAT production was most sensitive to parameters and initial conditions directly associated with CAT synthesis, as well as GTP/GMP synthesis, amino acid synthesis, and to a lesser extent amino acid initial conditions. On the other hand, CAT production was robust to allosteric control parameters and the initial conditions of glucose and oxygen.

The cell free model ensemble described the training data with the exception of some of the amino acids. Specifically, adding more reactions that consume amino acids would improve the model's ability to predict those that show a decrease in the experimental data. Also, including specific transcription and translation steps for CAT would allow us to more accurately model the complexity and the resource cost of protein synthesis. Another area for future work is to more thoroughly sample parameter space. For the metabolites in the dataset, initial conditions were fixed at the initial data values. All other parameters were varied in a manner so as to best fit the dataset. However, the resulting ensemble may not

represent every biological or practical possibility. In a different region of parameter space, the system could behave differently, including the flux distribution through the network, the accuracy and spread of ensemble fits, the relative sensitivities, and the yield as a percentage of the theoretical maximum. Testing the model under a variety of conditions could strengthen or challenge the findings of this study. Further experimentation could also be used to gain a deeper understanding of model performance under a variety of conditions. Specifically, CAT production performed in the absence of amino acids could inform the system's ability to manufacture them, while experimentation in the absence of glucose or oxygen could shed light on how important they are to protein synthesis, and under which conditions. Finally, the approach should be extended to other protein products. CAT is only a test protein used for model identification; the modeling framework, and to some extent the parameter values, should be protein agnostic. An important extension of this study would be to apply its insights to other protein applications, where possible.

Materials and Methods

Formulation and solution of the model equations We used ordinary differential equations (ODEs) to model the time evolution of metabolite (x_i) and scaled enzyme abundance (ϵ_i) in hypothetical cell-free metabolic networks:

$$\frac{dx_i}{dt} = \sum_{j=1}^{\mathcal{R}} \sigma_{ij} r_j(\mathbf{x}, \epsilon, \mathbf{k}) \quad i = 1, 2, \dots, \mathcal{M} \quad (1)$$

$$\frac{d\epsilon_i}{dt} = -\lambda_i \epsilon_i \quad i = 1, 2, \dots, \mathcal{E} \quad (2)$$

where \mathcal{R} denotes the number of reactions, \mathcal{M} denotes the number of metabolites and \mathcal{E} denotes the number of enzymes in the model. The quantity $r_j(\mathbf{x}, \epsilon, \mathbf{k})$ denotes the rate of reaction j . Typically, reaction j is a non-linear function of metabolite and enzyme abundance, as well as unknown kinetic parameters \mathbf{k} ($\mathcal{K} \times 1$). The quantity σ_{ij} denotes the stoichiometric coefficient for species i in reaction j . If $\sigma_{ij} > 0$, metabolite i is produced by reaction j . Conversely, if $\sigma_{ij} < 0$, metabolite i is consumed by reaction j , while $\sigma_{ij} = 0$ indicates metabolite i is not connected with reaction j . Lastly, λ_i denotes the scaled enzyme degradation constant. The system material balances were subject to the initial conditions $\mathbf{x}(t_o) = \mathbf{x}_o$ and $\epsilon(t_o) = 1$ (initially we have 100% cell-free enzyme abundance).

The reaction rate was written as the product of a kinetic term (\bar{r}_j) and a control term (v_j), $r_j(\mathbf{x}, \mathbf{k}) = \bar{r}_j v_j$. In this study, we used either saturation or mass action kinetics. The control term $0 \leq v_j \leq 1$ depended upon the combination of factors which influenced rate process j . For each rate, we used a rule-based approach to select from competing control factors. If rate j was influenced by $1, \dots, m$ factors, we modeled this relationship as $v_j = \mathcal{I}_j(f_{1j}(\cdot), \dots, f_{mj}(\cdot))$ where $0 \leq f_{ij}(\cdot) \leq 1$ denotes a regulatory transfer function quantifying the influence of factor i on rate j . The function $\mathcal{I}_j(\cdot)$ is an integration rule which maps the output of regulatory transfer functions into a control variable. Each regulatory

242 transfer function took the form:

$$f_{ij}(\mathcal{Z}_i, k_{ij}, \eta_{ij}) = k_{ij}^{\eta_{ij}} \mathcal{Z}_i^{\eta_{ij}} / (1 + k_{ij}^{\eta_{ij}} \mathcal{Z}_i^{\eta_{ij}}) \quad (3)$$

243 where \mathcal{Z}_i denotes the abundance factor i , k_{ij} denotes a gain parameter, and η_{ij} denotes
 244 a cooperativity parameter. In this study, we used $\mathcal{I}_j \in \{mean\}$ [?]. If a process has no
 245 modifying factors, $v_j = 1$. We used multiple saturation kinetics to model the reaction term
 246 \bar{r}_j :

$$\bar{r}_j = k_j^{max} \epsilon_i \left(\prod_{s \in m_j^-} \frac{x_s}{K_{js} + x_s} \right) \quad (4)$$

247 where k_j^{max} denotes the maximum rate for reaction j , ϵ_i denotes the scaled enzyme ac-
 248 tivity which catalyzes reaction j , and K_{js} denotes the saturation constant for species s
 249 in reaction j . The product in Equation (4) was carried out over the set of *reactants* for
 250 reaction j (denoted as m_j^-).

251 We added regulation to the network as informed by literature, for a total of 17 inter-
 252 actions. PEP was modeled as an inhibitor for phosphofructokinase [29, 30], PEP car-
 253 boxykinase [29], PEP synthetase [29, 31], isocitrate dehydrogenase [29, 32], and isoci-
 254 trate lyase/malate synthase [29, 32, 33], and as an activator for fructose-biphosphatase
 255 [29, 34–36]. AKG was modeled as an inhibitor for citrate synthase [29, 37, 38] and isoc-
 256 itrate lyase/malate synthase [29, 33]. 3PG was modeled as an inhibitor for isocitrate
 257 lyase/malate synthase [29, 33]. FDP was modeled as an activator for pyruvate kinase
 258 [29, 39] and PEP carboxylase [29, 40]. Pyruvate was modeled as an inhibitor for pyruvate
 259 dehydrogenase [29, 41, 42] and as an activator for lactate dehydrogenase [43]. Acetyl
 260 CoA was modeled as an inhibitor for malate dehydrogenase [29].

261 **Generation of model ensemble** We generated an ensemble of 100 diverse parameter
 262 sets via a Markov chain Monte Carlo random walk. Beginning with a single parameter

263 set as a starting point, we calculated its cost function, equal to the sum-squared-error
 264 between experimental data and model predictions:

$$cost = \sum_{i=1}^{\mathcal{D}} \left(w_i \sum_{j=1}^{\mathcal{T}_i} abs \left(x_{ij}^{data} - x_i^{sim}|_{t(j)} \right) \right) \quad (5)$$

265 where \mathcal{D} denotes the number of datasets, w_i denotes the weight of the i th dataset, \mathcal{T}_i
 266 denotes the number of timepoints in the i th dataset, $t(j)$ denotes the j th timepoint, x_{ij}^{data}
 267 denotes the value of the i th dataset at the j th timepoint, and $x_i^{sim}|_{t(j)}$ denotes the sim-
 268 ulated value of the metabolite corresponding to the i th dataset, interpolated to the j th
 269 timepoint. We then perturbed model parameters:

$$k_i^{new} = k_i * exp(a r_i) \quad i = 1, 2, \dots, \mathcal{P} \quad (6)$$

270 where \mathcal{P} denotes the number of parameters, equal to 815, which includes 163 rate con-
 271 stants, 163 enzyme degradation rate constants, 455 saturation constants, and 34 control
 272 parameters, k_i^{new} denotes the new value of the i th parameter, k_i denotes the current value
 273 of the i th parameter, a denotes a distribution variance, and r_i denotes a random sample
 274 from the normal distribution. For each newly generated parameter set, we re-solved the
 275 balance equations and calculated the cost function. All sets with a lower cost than the
 276 previous set, and some with higher cost, were added to the ensemble. After generating
 277 12,437 sets, we selected 100 sets with minimal correlation to each other so as to avoid
 278 over-sampling any region of parameter space. The original 12,437-set ensemble had
 279 a [mean,median,maximum] Pearson correlation coefficient [REFERENCE NEEDED?] of
 280 [?] between pairs of sets; the 100-set ensemble had a [mean,median,maximum] Pearson
 281 correlation coefficient of [?] between pairs of sets.

Local sensitivity analysis We determined the reactions most important to protein production by computing the local sensitivity of CAT concentration to each rate constant in the network. Each sensitivity index was formulated as:

$$S_{ij} = \text{norm}(CAT(p_i, p_j, t) - CAT(\alpha * p_i, \alpha * p_j, t)) \quad i, j = 1, 2, \dots \mathcal{P} \quad (7)$$

where S_{ij} denotes the sensitivity of CAT production to the i th and j th parameters, $CAT(p_i, p_j, t)$ denotes CAT concentration as a function of time and the i th and j th parameters, α denotes the perturbation factor, equal to 1.01, and \mathcal{P} denotes the number of rate constants, equal to 163. In calculating the pairwise sensitivities, each parameter was perturbed by 1%;

Sequence specific FBA and calculation of CAT yield The yield on CAT production was calculated for each case as a ratio of carbon produced as CAT to carbon consumed as reactants (glucose and amino acids):

$$Yield = \frac{\Delta CAT \ C_{CAT}}{\sum_{i=1}^{\mathcal{R}} \max(\Delta m_i, 0) \ C_{m_i}} \quad (8)$$

where ΔCAT denotes the amount of CAT produced, C_{CAT} denotes carbon number of CAT, \mathcal{R} denotes the number of reactants, Δm_i denotes the amount of the i th reactant consumed, never allowed to be negative, and C_{m_i} denotes the carbon number of the i th reactant. Because no data was available for arginine or glutamate, these reactants were left out of all three calculations. In the experimental case and the best-fit set case, yield was calculated by setting ΔCAT equal to the final minus the initial CAT concentration and setting Δm_i equal to the initial minus the final reactant concentration. The theoretical yield was calculated using flux balance analysis (FBA) with a sequence-specific based

analysis on CAT. The sequence specific FBA [44] problem was formulated as:

$$\max_{\mathbf{w}} (w_{obj} = \boldsymbol{\theta}^T \mathbf{w})$$

$$\text{Subject to : } \mathbf{S}\mathbf{w} = \mathbf{0}$$

$$\alpha_i \leq w_i \leq \beta_i \quad i = 1, 2, \dots, \mathcal{R}$$

where \mathbf{S} denotes the stoichiometric matrix, \mathbf{w} denotes the unknown flux vector, $\boldsymbol{\theta}$ denotes the objective selection vector and α_i and β_i denote the lower and upper bounds on flux w_i , respectively. The objective w_{obj} was to maximize the specific rate of CAT formation. The specific glucose uptake rate was constrained to allow a maximum flux of 40 mM/hr according to literature data; the specific amino acid uptake rates were also bound to allow a maximum flux of 30 mM/hr, but did not reach this maximum flux. The transcription and translation template reactions were added to the metabolic network and are based off sequence specific analysis [44] involving transcription initiation, transcription, mRNA degradation, translation initiation, translation, and tRNA charging. The mRNA and protein sequence of each protein was determined from literature. The transcription rate was constrained as:

$$w_{tx} = RNAP \frac{v_{RNAP}}{l_{mRNA}} \left(\frac{Gene}{km + Gene} \right) P$$

where $RNAP$ is the concentration of RNA polymerase, v_{RNAP} is the elongation rate (nucleotides/hr) by the RNA polymerase, l_{mRNA} is the number of nucleotides in the mRNA, $Gene$ is the gene concentration, km is the plasmid saturation coefficient, and P is the promoter activity.

The promoter activity was formulated following Moon et al. for synthetic circuits as:

$$P = \frac{K_1}{1 + K_1}$$

where K_1 represents the state of T7 RNA polymerase binding.

The translation rate was constrained as:

$$w_{tl} = K_P Ribo \frac{v_{Ribo}}{l_{protein}} [mRNA_{ss}]$$

where K_P is the polysome amplification constant, $Ribo$ is the ribosome concentration, v_{Ribo} is the elongation rate (amino acids/hr) of the ribosome, $l_{protein}$ is the number of amino acids in the protein of interest, and $mRNA_{ss}$ is the mRNA concentration at steady state determined by the transcription rate divided by the degradation rate of mRNA. An ensemble of flux distributions was calculated for 100 sets by randomly sampling. Glucose, oxygen, and amino acids were modeled as being imported into the system, whereas CAT synthesis and metabolite byproduct formation was modeled as an export from the system. The rest of the network followed a pseudo steady-state assumption where all other metabolites were not allowed to accumulate; thus, the network could be solved by linear programming. The flux balance analysis problem was solved using the GNU Linear Programming Kit (v4.52) [45]. The solution flux vector was used to calculate the theoretical carbon yield of CAT for four different cases. For the unconstrained case, all rates were left unbounded. An ensemble of flux distributions was calculated by randomly sampling the maximum specific glucose uptake rate from 30 to 40 mM/hr determined from experimental data. For the limited oxidative phosphorylation case, an ensemble of flux distributions was generated by randomly sampling the maximum specific oxygen uptake rate to from 0 to 10 mM/hr. For the TXTL case (constrained by transcription and translation rates), an ensemble was generated by randomly sampling RNAP polymerase levels, ribosome levels, and elongation rates in a physiological range determined from literature as well as the specific glucose uptake rate from 30 to 40 mM/hr. For the case where the flux was constrained by experimental data, the lower and upper bounds where data was available were

341 randomly sampled in the physiological range of the data in addition to randomly sampling
342 RNAP polymerase levels, ribosome levels, and elongation rates in a physiological range
343 determined from literature.

Funding

This study was supported by a National Science Foundation Graduate Research Fellowship (DGE-1333468) to N.H and by an award from the US Army and Systems Biology of Trauma Induced Coagulopathy (W911NF-10-1-0376) to J.V for the support of M.V.

References

1. Jewett MC, Calhoun KA, Voloshin A, Wu JJ, Swartz JR (2008) An integrated cell-free metabolic platform for protein production and synthetic biology. *Mol Syst Biol* 4: 220.
2. Matthaei JH, Nirenberg MW (1961) Characteristics and stabilization of dnaase-sensitive protein synthesis in e. coli extracts. *Proc Natl Acad Sci U S A* 47: 1580-8.
3. Nirenberg MW, Matthaei JH (1961) The dependence of cell-free protein synthesis in e. coli upon naturally occurring or synthetic polyribonucleotides. *Proc Natl Acad Sci U S A* 47: 1588-602.
4. Lu Y, Welsh JP, Swartz JR (2014) Production and stabilization of the trimeric influenza hemagglutinin stem domain for potentially broadly protective influenza vaccines. *Proc Natl Acad Sci U S A* 111: 125-30.
5. Hodgman CE, Jewett MC (2012) Cell-free synthetic biology: thinking outside the cell. *Metab Eng* 14: 261-9.
6. Fredrickson AG (1976) Formulation of structured growth models. *Biotechnol Bioeng* 18: 1481-6.
7. Domach MM, Leung SK, Cahn RE, Cocks GG, Shuler ML (1984) Computer model for glucose-limited growth of a single cell of escherichia coli b/r-a. *Biotechnol Bioeng* 26: 203-16.
8. Steinmeyer D, Shuler M (1989) Structured model for *Saccharomyces cerevisiae*. *Chem Eng Sci* 44: 2017 - 2030.
9. Wu P, Ray NG, Shuler ML (1992) A single-cell model for cho cells. *Ann N Y Acad Sci* 665: 152-87.
10. Castellanos M, Wilson DB, Shuler ML (2004) A modular minimal cell model: purine and pyrimidine transport and metabolism. *Proc Natl Acad Sci U S A* 101: 6681-6.
11. Atlas JC, Nikolaev EV, Browning ST, Shuler ML (2008) Incorporating genome-wide

dna sequence information into a dynamic whole-cell model of escherichia coli: application to dna replication. IET Syst Biol 2: 369-82.

12. Dhurjati P, Ramkrishna D, Flickinger MC, Tsao GT (1985) A cybernetic view of microbial growth: modeling of cells as optimal strategists. Biotechnol Bioeng 27: 1-9.

13. Kompala DS, Ramkrishna D, Jansen NB, Tsao GT (1986) Investigation of bacterial growth on mixed substrates: experimental evaluation of cybernetic models. Biotechnol Bioeng 28: 1044-55.

14. Kim JI, Song HS, Sunkara SR, Lali A, Ramkrishna D (2012) Exacting predictions by cybernetic model confirmed experimentally: steady state multiplicity in the chemostat. Biotechnol Prog 28: 1160-6.

15. Varner J, Ramkrishna D (1999) Metabolic engineering from a cybernetic perspective: aspartate family of amino acids. Metab Eng 1: 88-116.

16. Song HS, Morgan JA, Ramkrishna D (2009) Systematic development of hybrid cybernetic models: application to recombinant yeast co-consuming glucose and xylose. Biotechnol Bioeng 103: 984-1002.

17. Song HS, Ramkrishna D (2011) Cybernetic models based on lumped elementary modes accurately predict strain-specific metabolic function. Biotechnol Bioeng 108: 127-40.

18. Lewis NE, Nagarajan H, Palsson BØ (2012) Constraining the metabolic genotype-phenotype relationship using a phylogeny of in silico methods. Nat Rev Microbiol 10: 291-305.

19. Edwards JS, Palsson BØ (2000) The escherichia coli mg1655 in silico metabolic genotype: its definition, characteristics, and capabilities. Proc Natl Acad Sci U S A 97: 5528-33.

20. Feist AM, Henry CS, Reed JL, Krummenacker M, Joyce AR, et al. (2007) A genome-scale metabolic reconstruction for escherichia coli k-12 mg1655 that accounts for

1260 orfs and thermodynamic information. *Mol Syst Biol* 3: 121.

21. Oh YK, Palsson BØ, Park SM, Schilling CH, Mahadevan R (2007) Genome-scale reconstruction of metabolic network in *Bacillus subtilis* based on high-throughput phenotyping and gene essentiality data. *J Biol Chem* 282: 28791-9.
22. Feist AM, Herrgård MJ, Thiele I, Reed JL, Palsson BØ (2009) Reconstruction of biochemical networks in microorganisms. *Nat Rev Microbiol* 7: 129-43.
23. Ibarra RU, Edwards JS, Palsson BØ (2002) *Escherichia coli* K-12 undergoes adaptive evolution to achieve in silico predicted optimal growth. *Nature* 420: 186-9.
24. Schuetz R, Kuepfer L, Sauer U (2007) Systematic evaluation of objective functions for predicting intracellular fluxes in *Escherichia coli*. *Mol Syst Biol* 3: 119.
25. Hyduke DR, Lewis NE, Palsson BØ (2013) Analysis of omics data with genome-scale models of metabolism. *Mol Biosyst* 9: 167-74.
26. McCloskey D, Palsson BØ, Feist AM (2013) Basic and applied uses of genome-scale metabolic network reconstructions of *Escherichia coli*. *Mol Syst Biol* 9: 661.
27. Zomorodi AR, Suthers PF, Ranganathan S, Maranas CD (2012) Mathematical optimization applications in metabolic networks. *Metab Eng* 14: 672-86.
28. Calhoun KA, Swartz JR (2005) An economical method for cell-free protein synthesis using glucose and nucleoside monophosphates. *Biotechnology Progress* 21: 1146–1153.
29. Kotte O, Zaugg JB, Heinemann M (2010) Bacterial adaptation through distributed sensing of metabolic fluxes. *Mol Syst Biol* 6: 355.
30. Cabrera R, Baez M, Pereira HM, Caniuguir A, Garratt RC, et al. (2011) The crystal complex of phosphofructokinase-2 of *Escherichia coli* with fructose-6-phosphate: kinetic and structural analysis of the allosteric ATP inhibition. *J Biol Chem* 286: 5774–5783.
31. Chulavatnatol M, Atkinson DE (1973) Phosphoenolpyruvate synthetase from *Es-*

cherichia coli. Effects of adenylate energy charge and modifier concentrations. J Biol Chem 248: 2712–2715.

32. Ogawa T, Murakami K, Mori H, Ishii N, Tomita M, et al. (2007) Role of phosphoenolpyruvate in the NADP-isocitrate dehydrogenase and isocitrate lyase reaction in Escherichia coli. J Bacteriol 189: 1176–1178.

33. MacKintosh C, Nimmo HG (1988) Purification and regulatory properties of isocitrate lyase from Escherichia coli ML308. Biochem J 250: 25–31.

34. Donahue JL, Bownas JL, Niehaus WG, Larson TJ (2000) Purification and characterization of glpX-encoded fructose 1, 6-bisphosphatase, a new enzyme of the glycerol 3-phosphate regulon of Escherichia coli. J Bacteriol 182: 5624–5627.

35. Hines JK, Fromm HJ, Honzatko RB (2006) Novel allosteric activation site in Escherichia coli fructose-1,6-bisphosphatase. J Biol Chem 281: 18386–18393.

36. Hines JK, Fromm HJ, Honzatko RB (2007) Structures of activated fructose-1,6-bisphosphatase from Escherichia coli. Coordinate regulation of bacterial metabolism and the conservation of the R-state. J Biol Chem 282: 11696–11704.

37. Pereira DS, Donald LJ, Hosfield DJ, Duckworth HW (1994) Active site mutants of Escherichia coli citrate synthase. Effects of mutations on catalytic and allosteric properties. J Biol Chem 269: 412–417.

38. Robinson MS, Easom RA, Danson MJ, Weitzman PD (1983) Citrate synthase of Escherichia coli. Characterisation of the enzyme from a plasmid-cloned gene and amplification of the intracellular levels. FEBS Lett 154: 51–54.

39. Zhu T, Bailey MF, Angley LM, Cooper TF, Dobson RC (2010) The quaternary structure of pyruvate kinase type 1 from Escherichia coli at low nanomolar concentrations. Biochimie 92: 116–120.

40. Wohl RC, Markus G (1972) Phosphoenolpyruvate carboxylase of Escherichia coli. Purification and some properties. J Biol Chem 247: 5785–5792.

- 452 41. Kale S, Arjunan P, Furey W, Jordan F (2007) A dynamic loop at the active center
453 of the Escherichia coli pyruvate dehydrogenase complex E1 component modulates
454 substrate utilization and chemical communication with the E2 component. J Biol
455 Chem 282: 28106–28116.
- 456 42. Arjunan P, Nemeria N, Brunskill A, Chandrasekhar K, Sax M, et al. (2002) Structure of
457 the pyruvate dehydrogenase multienzyme complex E1 component from Escherichia
458 coli at 1.85 Å resolution. Biochemistry 41: 5213–5221.
- 459 43. Okino S, Suda M, Fujikura K, Inui M, Yukawa H (2008) Production of D-lactic acid by
460 Corynebacterium glutamicum under oxygen deprivation. Appl Microbiol Biotechnol
461 78: 449–454.
- 462 44. Allen TE, Palsson BØ (2003) Sequence-based analysis of metabolic demands for
463 protein synthesis in prokaryotes. Journal of Theoretical Biology 220: 1 - 18.
- 464 45. (2016). GNU Linear Programming Kit, Version 4.52. URL [http://www.gnu.org/
465 software/glpk/glpk.html](http://www.gnu.org/software/glpk/glpk.html).

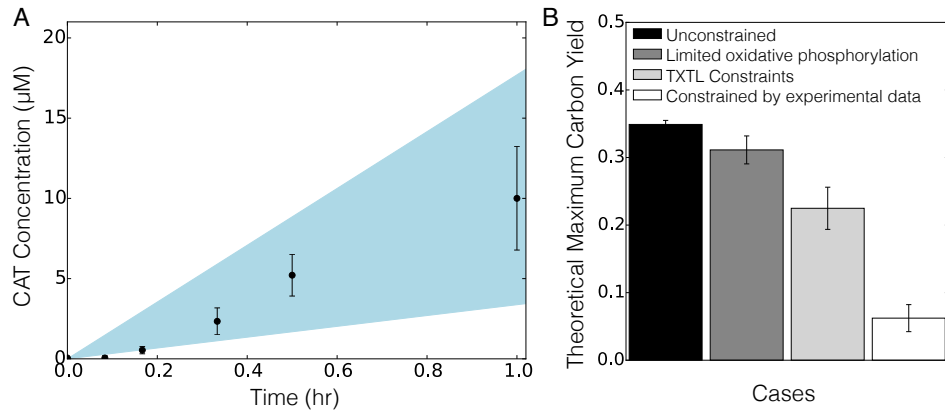


Fig. 1: Sequence specific flux balance analysis of CAT production and yield. A. 95% confidence interval of the ensemble (light blue region) for CAT concentration versus time. B. Theoretical maximum carbon yield of CAT calculated by ssFBA for four different cases: unconstrained (black), limited oxidative phosphorylation activity (gray), constrained by transcription and translation rates (light grey), and constrained by experimental data (white). Error bars represent standard deviation of the ensemble.

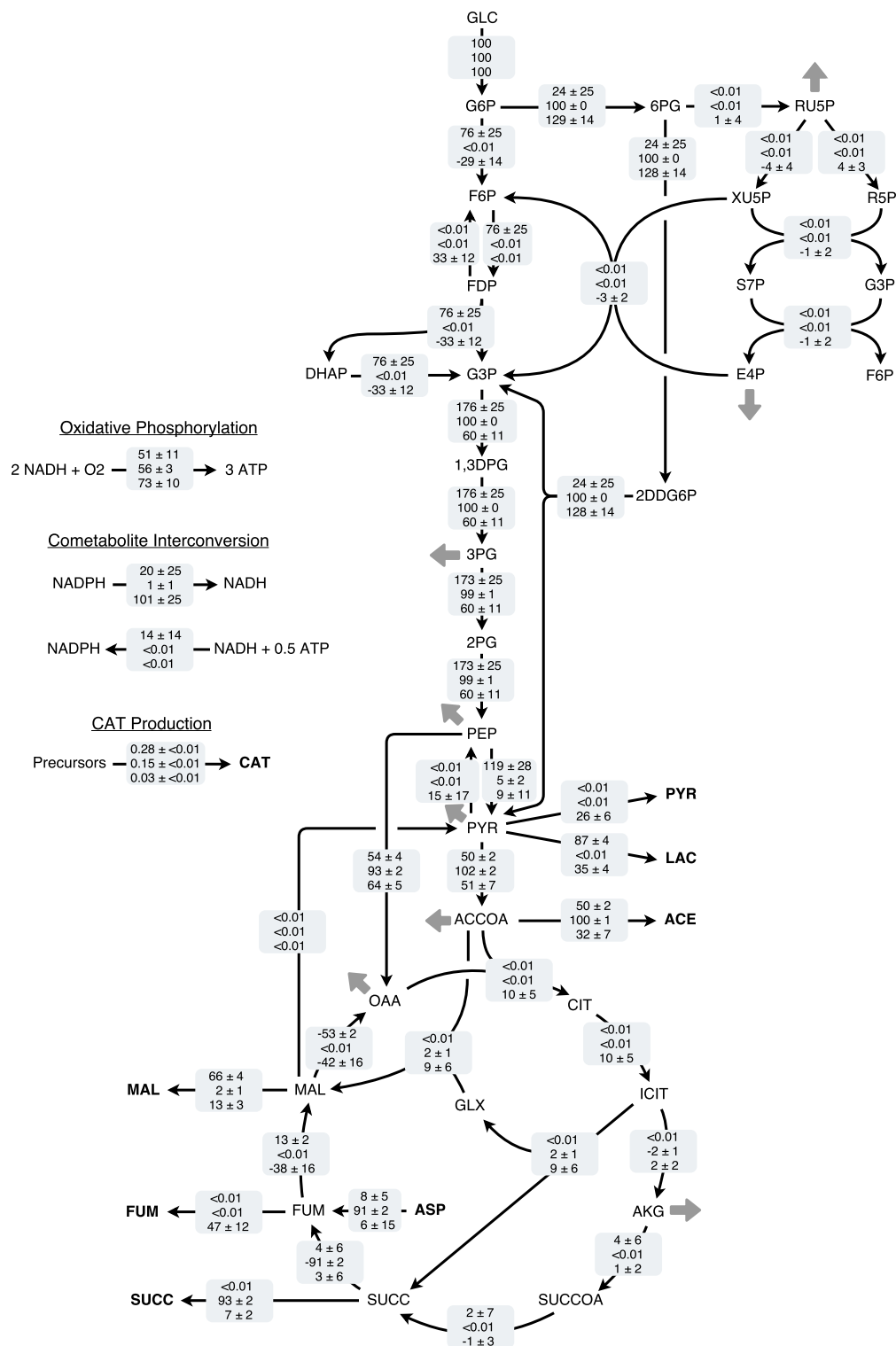


Fig. 2: Flux profile for glycolysis, pentose phosphate pathway, Entner-Doudoroff pathway, TCA cycle, NADPH/NADH transfer, and oxidative phosphorylation. Sequence specific FBA flux value (mean ± standard deviation) across ensemble for 1 hr, normalized to glucose uptake flux. Unconstrained (top row), constrained by transcription and translation rates (second row), and constrained by experimental data (bottom row) shows the flux distribution throughout central carbon metabolism.

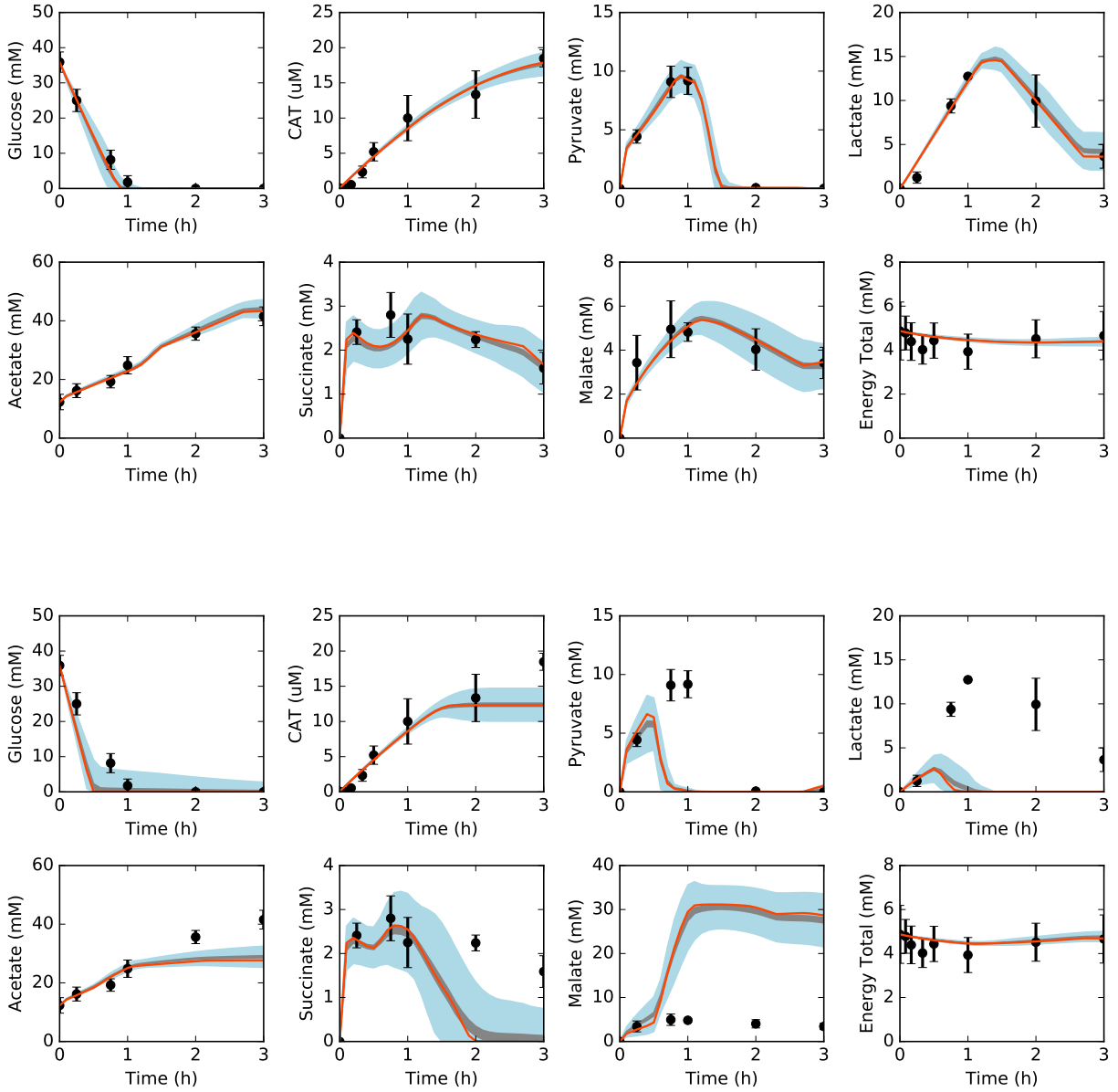


Fig. 3: Central carbon metabolism in the presence (top) and absence (bottom) of allosteric control, including glucose (substrate), CAT (product), and intermediates, as well as total concentration of energy species. Best-fit parameter set (orange line) versus experimental data (points). 95% confidence interval (blue shaded region) and 95% confidence interval of the mean (gray shaded region) over the ensemble of 100 sets.

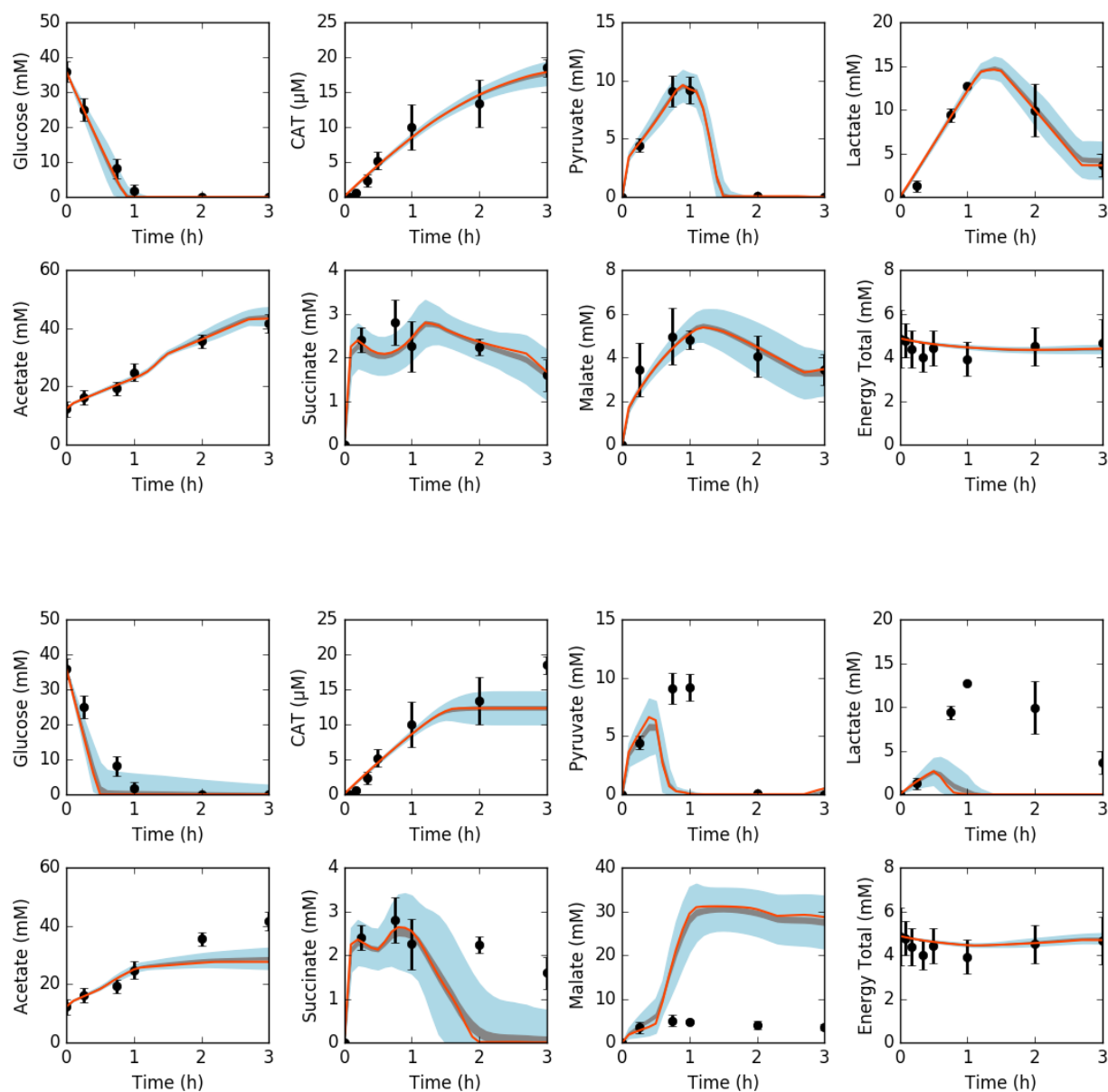


Fig. 4: Central carbon metabolism in the presence (top) and absence (bottom) of allosteric control, including glucose (substrate), CAT (product), and intermediates, as well as total concentration of energy species. Best-fit parameter set (orange line) versus experimental data (points). 95% confidence interval (blue shaded region) and 95% confidence interval of the mean (gray shaded region) over the ensemble of 100 sets.

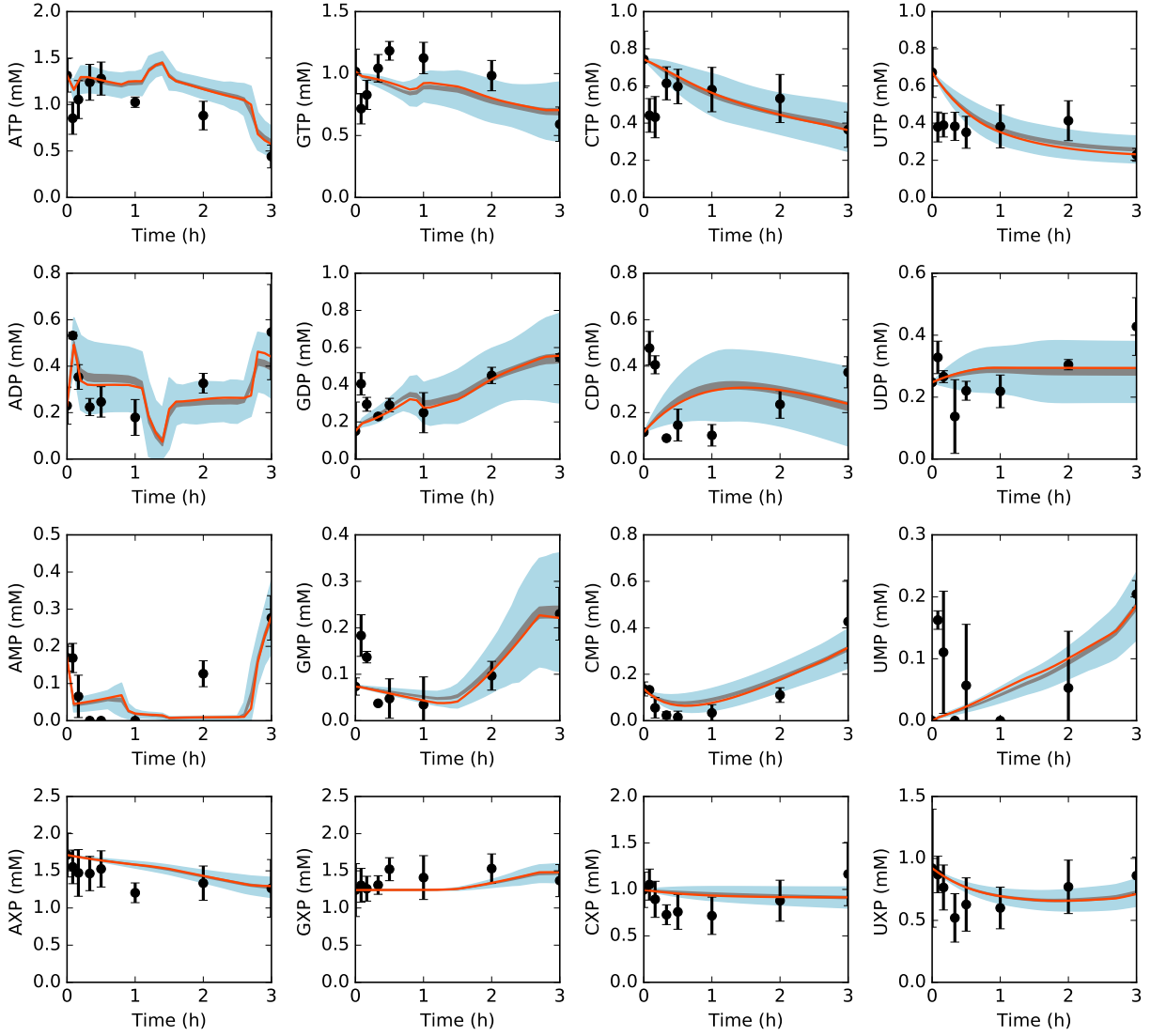


Fig. 5: Energy species and energy totals by base in the presence of allosteric control. Best-fit parameter set (orange line) versus experimental data (points). 95% confidence interval (blue shaded region) and 95% confidence interval of the mean (gray shaded region) over the ensemble of 100 sets.

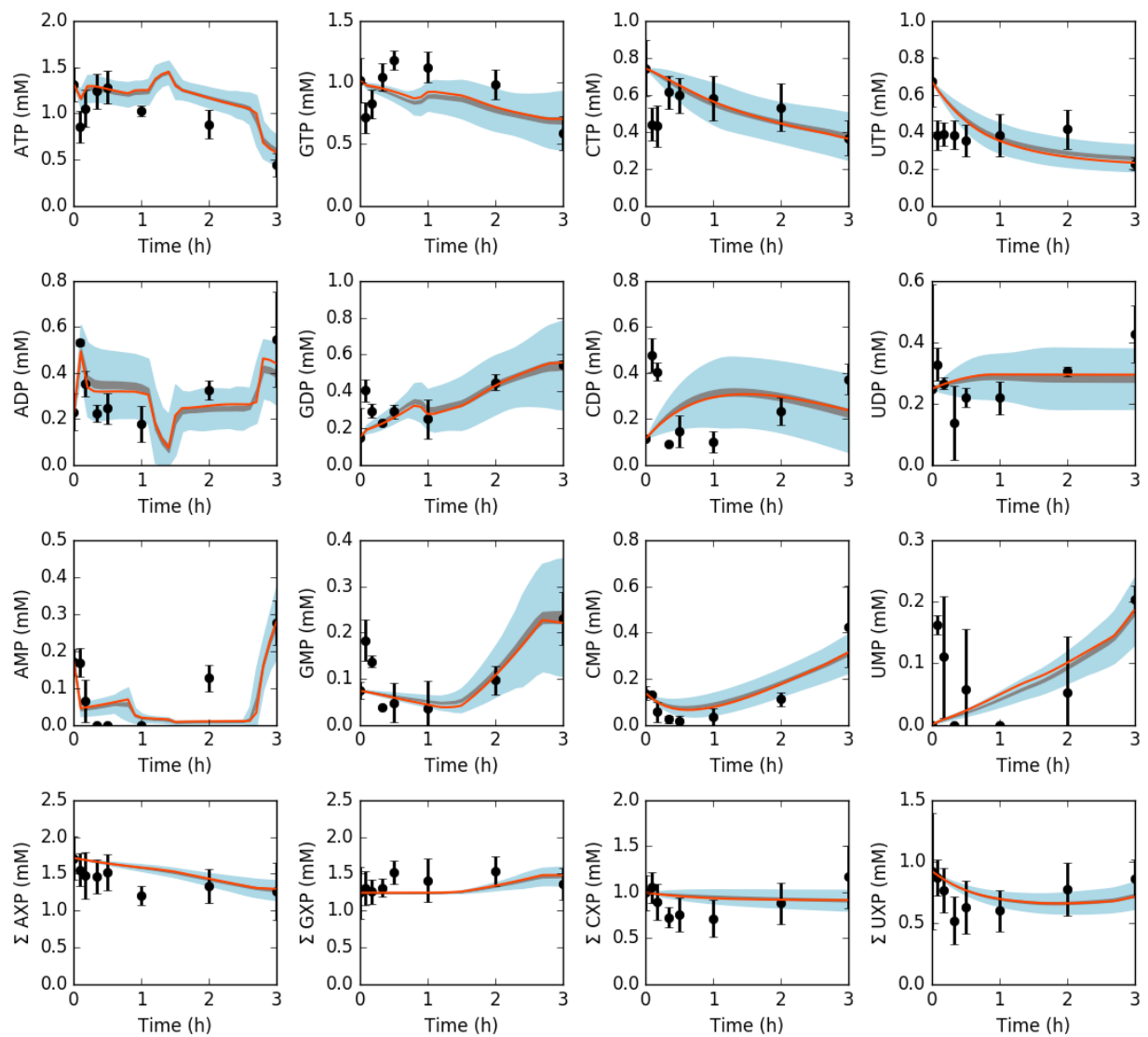


Fig. 6: Energy species and energy totals by base in the presence of allosteric control. Best-fit parameter set (orange line) versus experimental data (points). 95% confidence interval (blue shaded region) and 95% confidence interval of the mean (gray shaded region) over the ensemble of 100 sets.

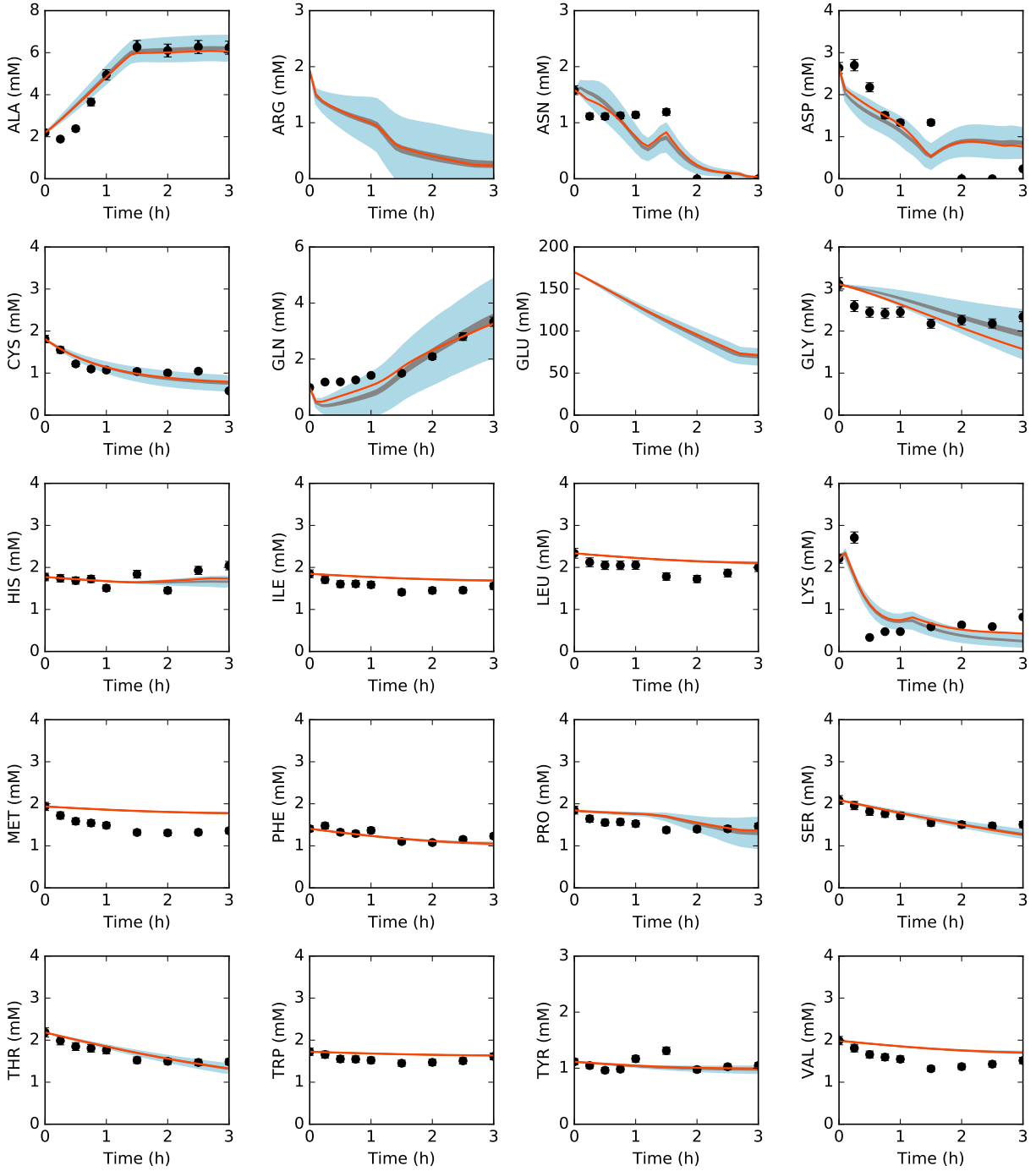


Fig. 7: Amino acids in the presence of allosteric control. Best-fit parameter set (orange line) versus experimental data (points). 95% confidence interval (blue shaded region) and 95% confidence interval of the mean (gray shaded region) over the ensemble of 100 sets.

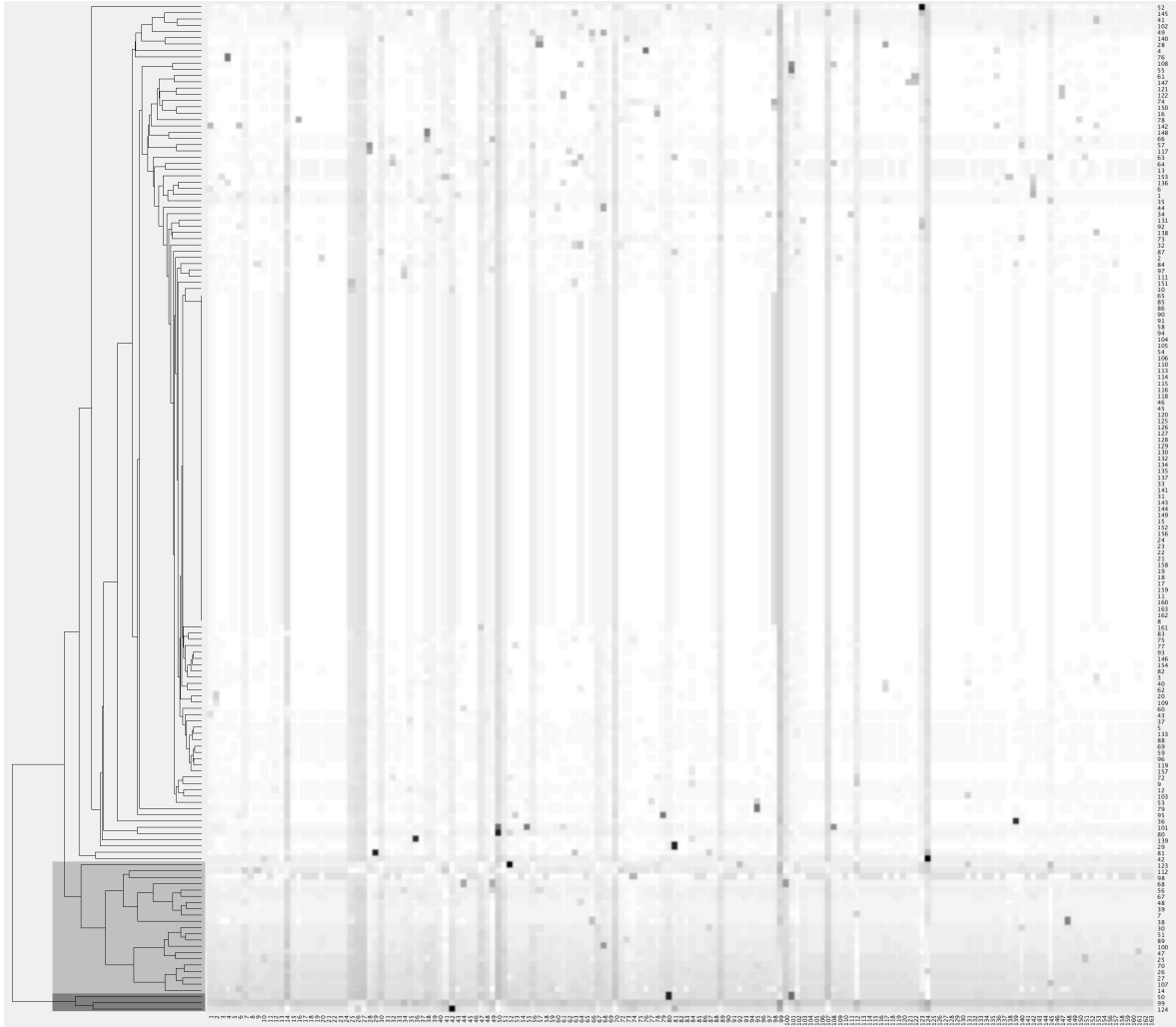


Fig. 8: Normalized first-order and pairwise sensitivities of CAT production to rate constants. Dark pixels indicate the most sensitive indices. Dendrogram indicates high responders (dark gray background), medium responders (medium gray background), and low responders (light gray background).

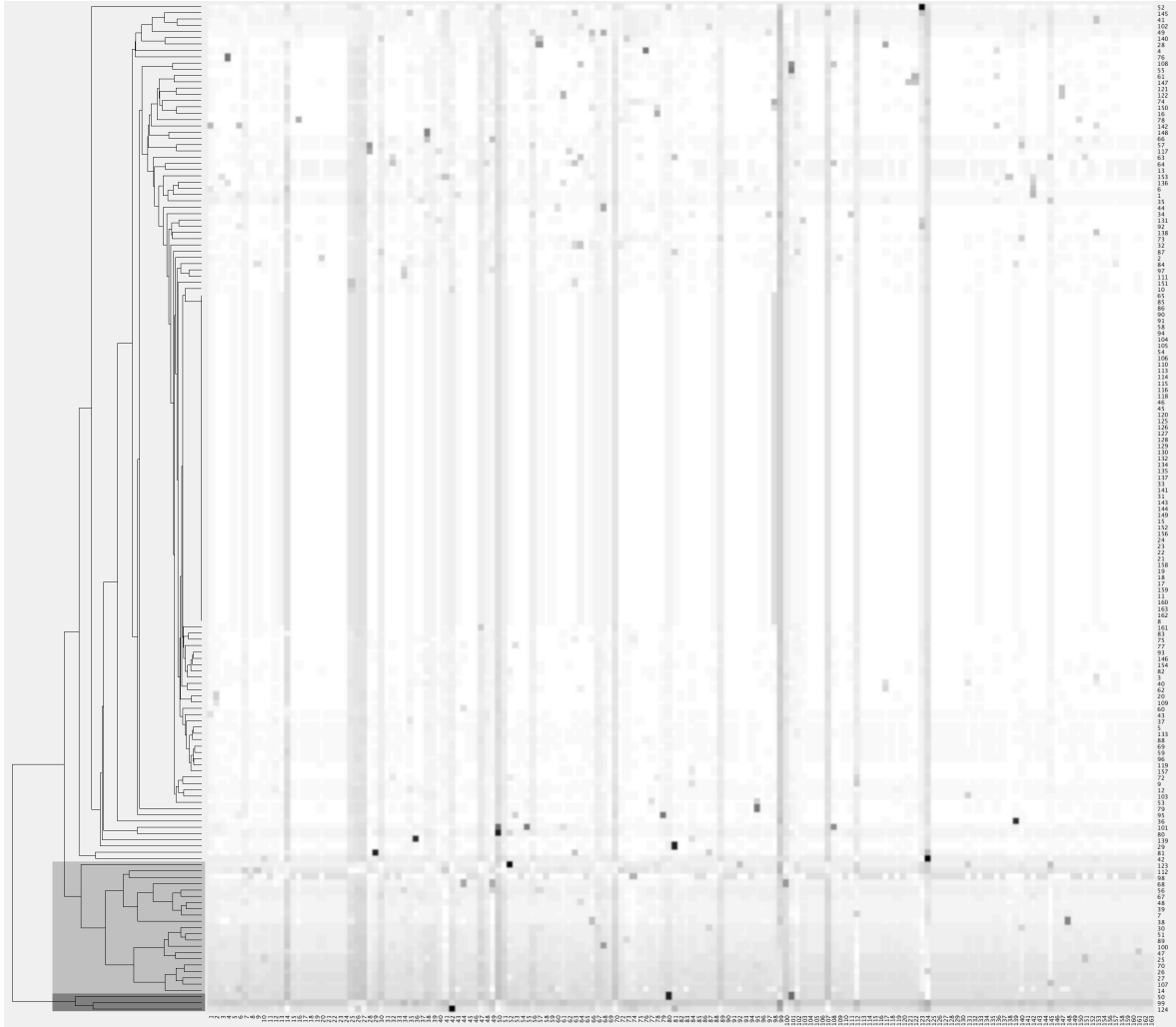


Fig. 9: Normalized first-order and pairwise sensitivities of CAT production to rate constants. Dark pixels indicate the most sensitive indices. Dendrogram indicates high responders (dark gray background), medium responders (medium gray background), and low responders (light gray background).



Fig. 10: Normalized first-order and pairwise sensitivities of system state to rate constants. Dark pixels indicate the most sensitive indices. Dendrogram indicates high responders (dark gray background), medium responders (medium gray background), and low responders (light gray background).

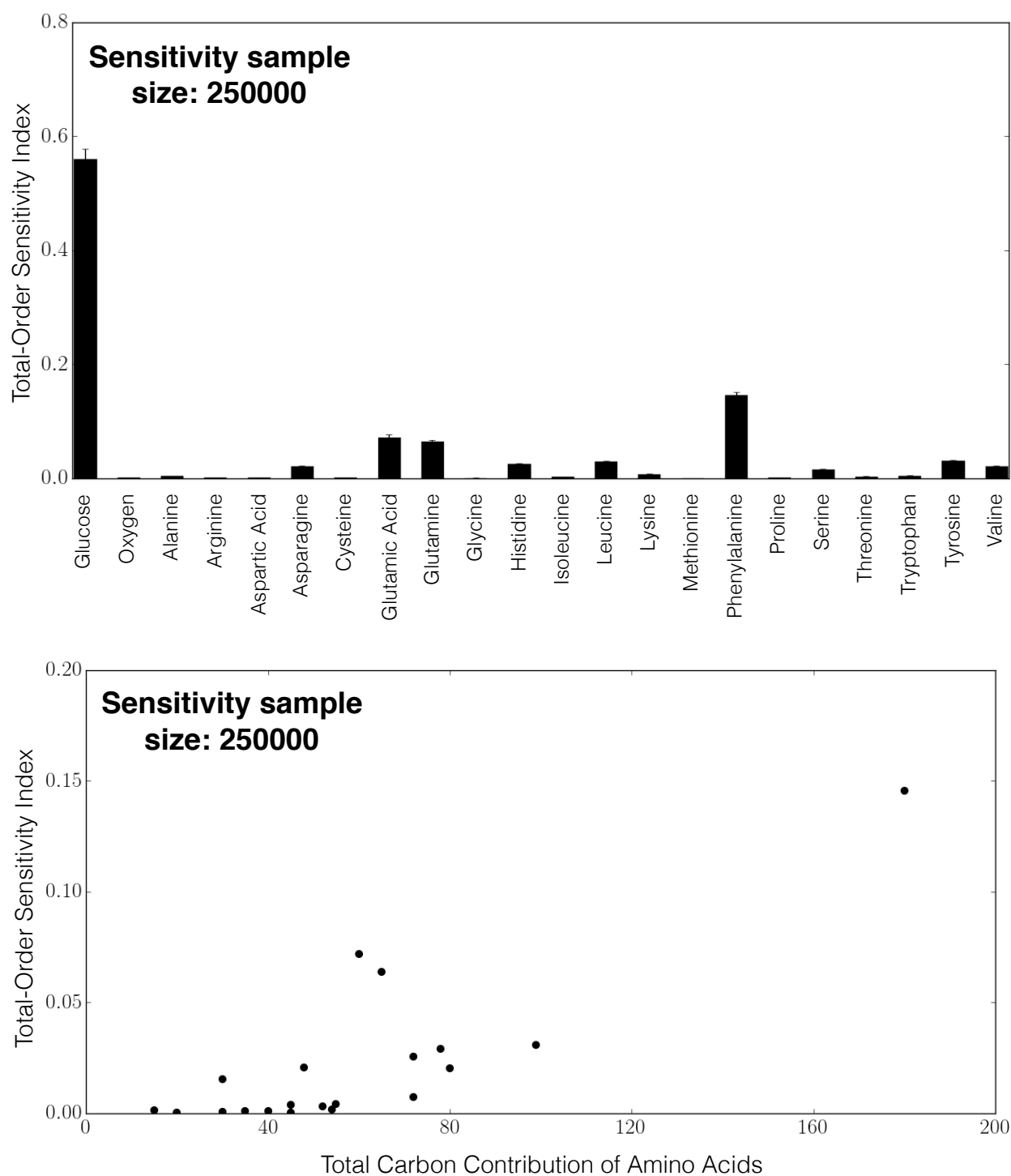


Fig. 11: Total-order global sensitivities of protein export flux to amino acid import flux upper bounds. Each upper bound was varied from 0 to 0.5 mM/hr.

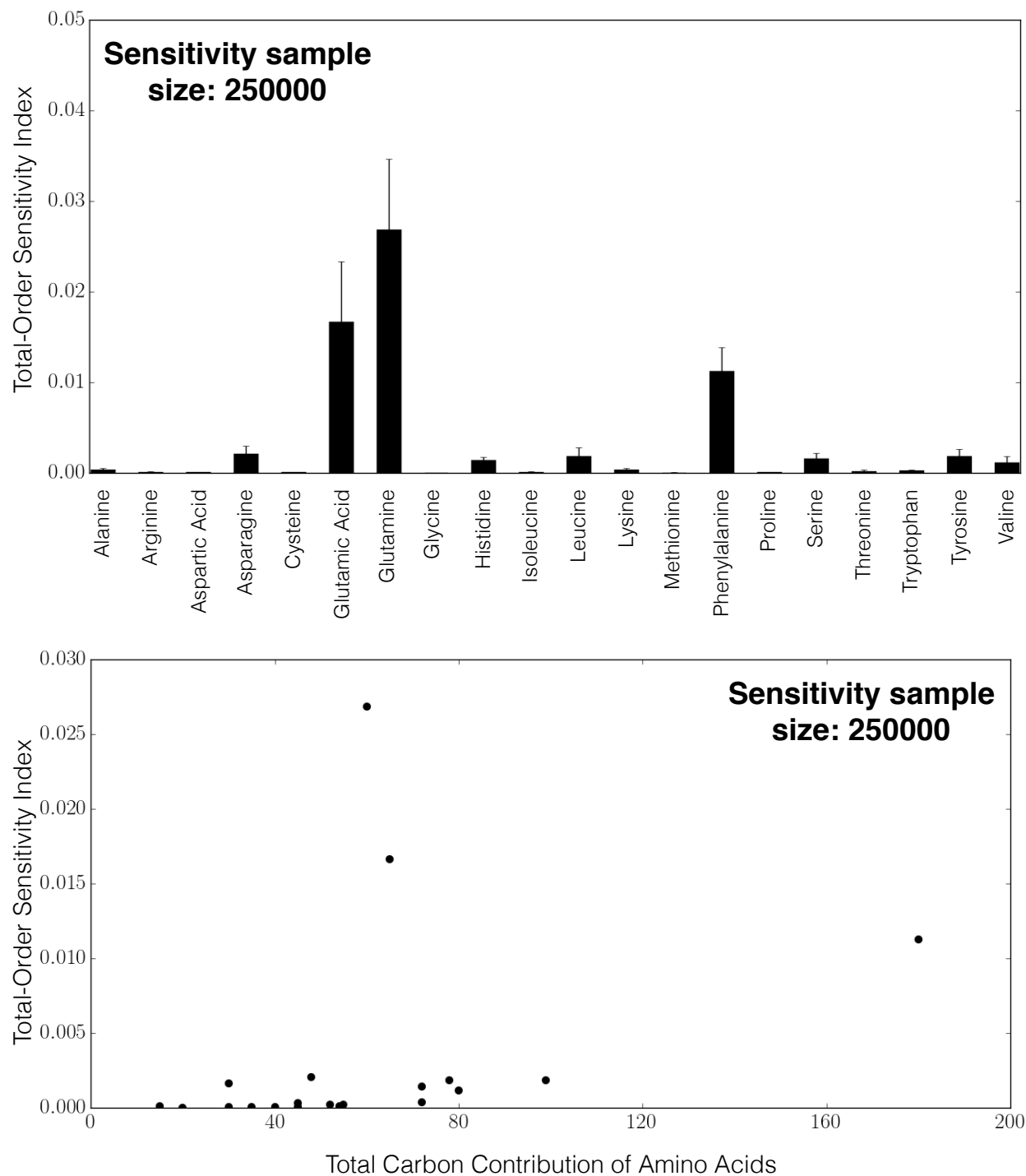


Fig. 12: Total-order global sensitivities of protein export flux to amino acid import flux upper bounds. Each upper bound was varied from 0 to 0.5 mM/hr, except the upper bound with respect to which sensitivity was calculated; this was varied from 0 to 10 mM/hr.

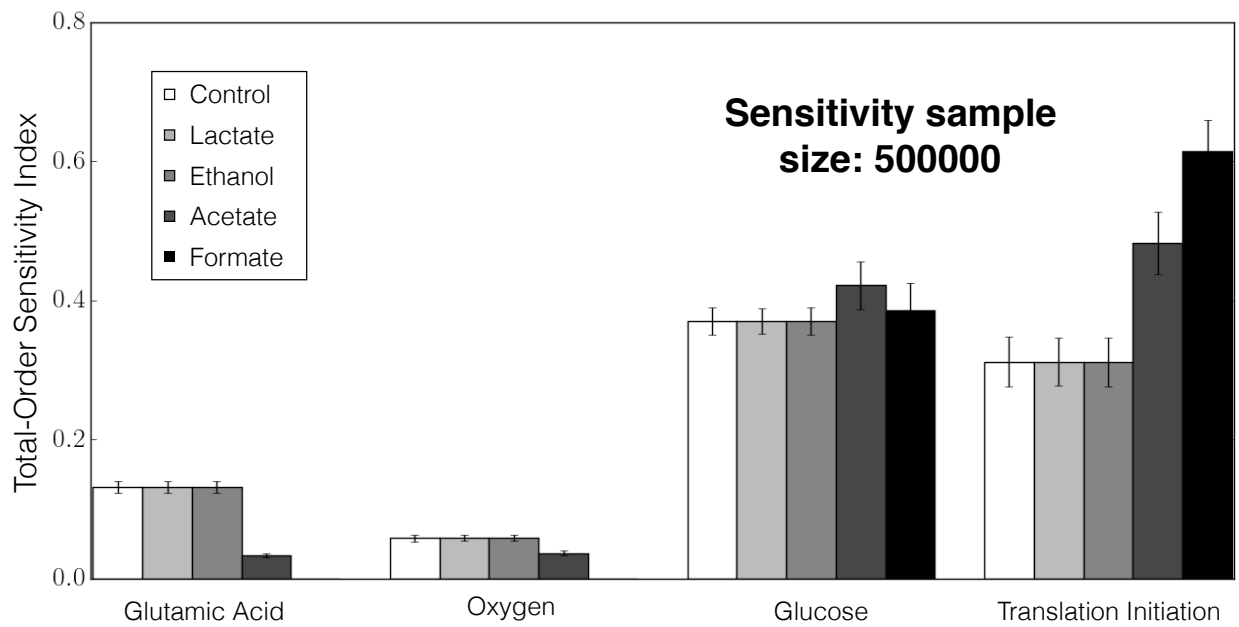


Fig. 13: Total-order global sensitivities of protein export flux to glutamic acid, oxygen and glucose import flux upper bounds, and translation initiation rate upper bound. Lactate, ethanol, acetate, and formate export fluxes were held constant at 0.1 mM/hr in the control case. One of these export fluxes was held constant at 10 mM/hr, while the others were held constant at 0.1 mM/hr, in each of the other four cases.